Electronic Supplementary Material (ESI) for Journal of Materials Chemistry A.

Supplementary Information

Zn_2GeO_4 and Zn_2SnO_4 Nanowires for High-Capacity Lithium- and Sodium-Ion Batteries

Young Rok Lim,[a] Chan Su Jung,[a] Hyung Soon Im,[a] Kidong Park,[a] Jeunghee Park,*[a] Won Il Cho[b] and Eun Hee Cha*[c]

[a] *Department of Chemistry, Korea University, Jochiwon 339-700, Korea; parkjh@korea.ac.kr*

[b]*Center for Energy Convergence, Korea Institute of Science and Technology, Seoul 136-791, Korea; wonic@kist.re.kr*

[c]*Department of Pharmaceutical Engineering, Hoseo University, Asan, Chungnam 336-795, Korea; chaeunhee@hoseo.edu*

Contents

Reaction Mechanism

For the synthesis of Zn_2GeO_4 in water, the reaction equation can be

$GeO_2 + 2Zn^{2+} + 2H_2O \rightarrow Zn_2GeO_4 + 4H^+$ (1).

In the case of Zn_2SnO_4, 0.5 M NaOH was used. Therefore, $ZnSn(OH)_6$ phase will produce first (shown in Eq. 2), and the additional Zn^{2+} will react with OH^- and produce $Zn(OH)_4^{2-}$ phase (Eq. 3). With the increase of temperature and duration time, Zn_2SnO_4 phase will produce via Eq. 4,

$Zn^{2+} + Sn^{4+} + 6OH^- \rightarrow ZnSn(OH)_6$ (2)

$Zn^{2+} + 4OH^- \rightarrow Zn(OH)_4^{2-}$ (3)

$ZnSn(OH)_6 + Zn(OH)_4^{2-} \rightarrow Zn_2SnO_4 + 4H_2O + 2OH^-$ (4)

It is well-known that alkylamines (En) display bifunctionalities that mediate the crystal structure growth and control the 1D morphology of II-VI semiconductor and inorganic-organic hybrids because they can adsorb on solid surfaces and selectively bind to some specific panels to control the velocity and direction of crystal growth; this has been called the solvent-coordination molecular template mechanism. Therefore, we believe that the nanowire formation mainly originate from the structure-directing and regulating role of En through coordination and H-bonding interactions between the amino groups of En and the surface Zn, Ge (or Sn), and O moieties of the Zn_2GeO_4 or the Zn_2SnO_4 framework [cited from Ref. 56].

Table S1. Surface area of Zn_2GeO_4 and Zn_2SnO_4 (mixed with RGO) samples derived from the N_2 adsorption-desorption isotherms.

Sample	S_{BET}(m^2/g)[a]	V_{BJH}(cm^3/g)[b]
Zn_2GeO_4	41.00	0.851
Zn_2SnO_4	60.16	0.191

[a] Brunauer-Emmett-Teller (BET) specific surface area; [b] Barrett-Joyner-Halenda (BJH) model pore volume

N_2 adsorption-desorption isotherms were measured at 77 K on a Micromeritics Tristar 3000 analyzer, as shown below. Before the measurements, the sample was degassed at 300 ºC for 6 h. The specific surface area was calculated via the Brunauer-Emmett-Teller (BET) model at relative pressures of $P/P_0 = 0.20$. The total pore volume was estimated from the uptake of adsorbate at a relative pressure of $P/P_0 = 0.99$.

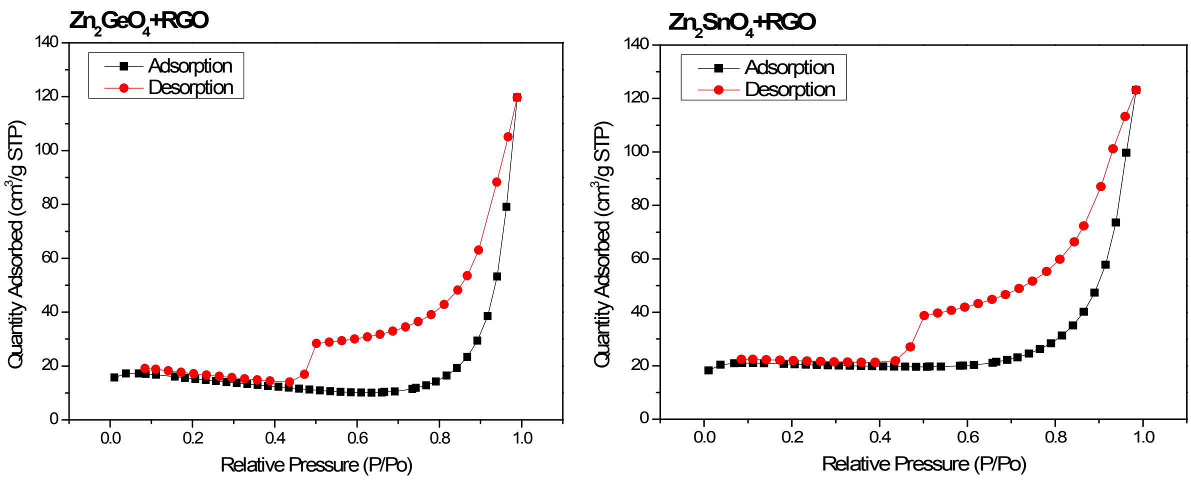

Table S2. Comparison of the electrochemical performance of Zn_2GeO_4 nanostructures in LIBs.

No.	Materials	Electrolyte/ additives	Potential (V)	First discharge capacity (mA h g^{-1})	Columbic efficiency in first cycle	Capacity after *x* cycles (mA h g^{-1})	References[a]
1	Zn_2GeO_4 nanorods	1M $LiPF_6$ EC:EMC:DMC=1:1:1v/v	0 - 3	1820	32 %	616 after 100 cycles	14
2	Zn_2GeO_4 amorphous nanoparticles	1M $LiPF_6$ EC:DEC:DMC+10% FEC =2:1:2 v/v	0 - 3	1619	34 %	1250 after 500 cycles	15
3	Zn_2GeO_4 nanorods @N-doped graphene	1M $LiPF_6$ EC:DEC=1:1 v/v	0.001 – 3	1463	60 %	1044 after 100 cycles	16
4	Zn_2GeO_4 nanowires	1M $LiPF_6$ EC:DEC=1:1 v/v	0.01 – 3	2320	39 %	1080 after 100 cycles	17
5	Zn_2GeO_4 nanorods @graphene oxide	1M $LiPF_6$ EC:DEC:DMC=1:1:1 Wt%	0.001 – 3	N/A[b]	N/A	1155 after 100 cycles	18
6	Zn_2GeO_4 nanorods @graphene	[c]N/A	0.01 – 3	1508	67.6	768 after 50 cycles	S2
7	Zn_2GeO_4 nanowires @carbon	1M $LiPF_6$ EC:DMC=1:1 v/v	0.01 – 3	1827	N/A	1112 after 50 cycles	19
8	Carbon-coated Zn_2GeO_4 on Ni foam	1M $LiPF_6$ EC:DMC=1:1 v/v	0.01 – 3	N/A	N/A	1128 after 1000 cycles	20
9	Zn_2GeO_4 nanoparticles@g-C_3N_4	1M $LiPF_6$ EC:DMC=1:1 v/v	0.001 – 3	1068	58.6	1300 after 140 cycles	21
10	Zn_2GeO_4 hollow nanoparticles	1M $LiPF_6$ EC:DMC=1:1 v/v	0.01 – 3	1587	56	1175 after 60 cycles	22
11	Mn-doped Zn_2GeO_4 hierarchical nanosheets	1M $LiPF_6$ EC:DEC=1:1 v/v	0.01 – 2	N/A	61.3	1301 after 100 cycles	23
12	Ag@C coated Zn_2GeO_4 nanorods	1M $LiPF_6$ EC:DMC=1:1 v/v	0 – 3	N/A	N/A	561 after 50 cycles	S3

13	Porous Zn_2GeO_4 nanofibers	1M $LiPF_6$ EC:DEC:DMC=1:1:1v/v	0.01 − 3	1705.6	82.4	1084.1 after 50 cycles	S4
14	Zn_2GeO_4@C nanofibers	1M $LiPF_6$ EC:DMC=1:1 v/v	0.005 – 2.9	1679.7	67	820 after 2000 cycles	S5

[a]Number corresponds to the references in the text; [b]N/A = not applicable.

Table S3. Comparison of the electrochemical performance of Zn_2SnO_4 nanostructures in LIBs.

No.	Materials	Electrolyte/ additives	Potential (V)	First discharge capacity (mA h g^{-1})	Columbic efficiency in first cycle	Capacity after *x* cycles (mA h g^{-1})	References[a]
1	Zn_2SnO_4 nanoparticles	1M $LiPF_6$ EC:PC:DMC=6:3:1 v/v	0.05 – 3	1509	N/A[b]	580 after 50 cycles	24
2	Zn_2SnO_4 particles	1M $LiClO_4$ EC:DMC=1:1 v/v	0.05 – 3	1903.6	N/A	644.7 after 20 cycles	25
3	Zn_2SnO_4 particles	1M $LiPF_6$ EC:DEC=1:1 v/v	0.05 – 3	2054	49.9	689 after 50 cycles	26
4	Zn_2SnO_4@C nanoparticles	1M $LiPF_6$ EC:EMC:DMC=1:1:1 v/v	0.05 – 3	1436.8	N/A	563.5 after 40 cycles	S6
5	Zn_2SnO_4 powders	1M $LiPF_6$ EC:DEC=1:1 v/v	0.05 – 3	1526	N/A	856 after 50 cycles	27
7	Zn_2SnO_4 nanoparticles	1M $LiPF_6$ EC:EMC:DMC=1:1:1 v/v	0.05 – 3	1512.7	N/A	503.7 after 40 cycles	S7
8	Zn_2SnO_4 cubes	1M $LiPF_6$ EC:EMC:DMC=1:1:1 v/v	0.05 – 3	1437	N/A	775 after 20 cycles	28
9	Zn_2SnO_4 nanoparticles	1M $LiPF_6$ EC:DEC=1:1 v/v	0.05 – 3	1773.2	52.8	521.4 after 40 cycles	S8
10	Zn_2SnO_4 nanoparticles	1M $LiPF_6$ EC:EMC:DMC=1:1:1 v/v	0.01 – 3	1323.8	N/A	349.2 after 20 cycles	S9
11	Zn_2SnO_4 particles @graphene	1M $LiPF_6$ EC:DMC=1:1 v/v	0.005 - 3	1521	N/A	326 after 50 cycles	S10
12	Zn_2SnO_4 nanoparticles	1M $LiPF_6$ EC:EMC:DMC=1:1:1	0.05 – 3	1670.8	41.8	342.7after 40 cycles	S11

		v/v					
13	Zn_2SnO_4 boxes	1M $LiPF_6$ EC:DEC:DMC=1:1:1 v/v	0.01 – 2	1554.8	56.8	540 after 45 cycles	S12
14	Zn_2SnO_4 nanowires	1M $LiPF_6$ EC:DMC=1:1 v/v	0.005 - 3	1650	N/A	660 after 50 cycles	29
15	Zn_2SnO_4 nanoparticles @graphene	1M $LiPF_6$ EC:DMC=1:1 v/v	0.005 – 3	1685	N/A	688 after 50 cycles	30
16	Zn_2SnO_4 hollow boxes @graphene	1M $LiPF_6$ EC:DEC:DMC=1:1:1 v/v	0.01 – 2	1624.7	69	752 after 45 cycles	31
17	Polyaniline coated Zn_2SnO_4 cubes	1M $LiPF_6$ EC:DEC:DMC=1:1:1 v/v	0.01 – 2	1795	N/A	491 after 50 cycles	S13
18	Zn_2SnO_4 boxes @C/graphene	1M $LiPF_6$ EC:DEC:DMC=1:1:1 v/v	0.01 – 2	1863	57	726.9 after 50 cycles	32
19	Zn_2SnO_4 nanoparticles	1M $LiPF_6$ EC:EMC:DMC=1:1:1 v/v	0.01 – 3	1629.9	56.98	642.2 after 20 cycles	33
20	Zn_2SnO_4 hollow boxes@graphene	1M $LiPF_6$ EC:DEC:DMC=1:1:1 v/v	0.01 – 2	1649.5	62	678.2 after 45 cycles	34
21	Zn_2SnO_4 flower like composites	1M $LiPF_6$ EC:DEC:DMC=1:1:1 v/v	0.01 – 2	1750	N/A	501 after 50 cycles	S14
22	Zn_2SnO_4 hollow nanospheres	1M $LiPF_6$ EC:DEC:DMC=1:1:1 v/v	0.01 – 3	1618.2	66.2	602.5 after 60 cycles	35
23	polypyrrole-coated Zn_2SnO_4 hollow Boxes	1M $LiPF_6$ EC:DEC:DMC=1:1:1 v/v	0.01 – 3	1105.2	50.3	478.4 after 50 cycles	S15
24	carbon coated Zn_2SnO_4	1M $LiPF_6$	0.05 – 3	1248.8	66.92	341after 45 cycles	S16

	nanoparticles	EC:DEC=1:1 v/v					
25	Zn_2SnO_4 nanoflowers @graphene	1M $LiPF_6$ EC:DMC:DEC=1:1:1 v/v	0.01 – 2	1967	55.3	540 after 50 cycles	S17
26	Zn_2SnO_4 hollow boxes @N–doped C	1M $LiPF_6$ EC:DMC:DEC=1:1:1 v/v	0.01 – 2	N/A	N/A	616 after 45 cycles	36
27	Zn_2SnO_4 core–shell nanorods@C	1M $LiPF_6$ EC:PC:DEC=3:1:1 v/v	0 – 2	1530	53.6	495 after 100 cycles	S18
28	Zn_2SnO_4 particles @mesoporous carbon	1M $LiPF_6$ EC:DMC=1:1 v/v	0.05 – 3	N/A	N/A	397 1920 mA/g	S19
30	Zn_2SnO_4 nanoparticles @graphene	1M $LiPF_6$ EC:EMC:DMC=1:1:1 v/v	0.01 – 3	1226	57.4	745 after 100 cycles	37
31	carbon coated Zn_2SnO_4 nanoparticles	1.3 M $LiPF_6$ EC:EMC=3:7 + 15% FEC	0.01 – 3	1454	66.36	467 after 50 cycles	S20
32	Co-doped Zn_2SnO_4 nanoparticles@graphene-C	1M $LiPF_6$ EC:EMC:DMC=1:1:1 v/v	0.01 – 3	1260	62.3	699 after 50 cycles	38
33	Zn_2SnO_4@carbon nanotubes	1M $LiPF_6$ EC:DMC=1:1 v/v	0.005 – 3	1925.4	55.31	703.8 after 30 cycles	S21

[a]Number corresponds to the references in the text; [b]N/A = not applicable.

Table S4. Equivalent circuit and impedance parameters from the LIBs and SIBs using Zn_2GeO_4 and Zn_2SnO_4.

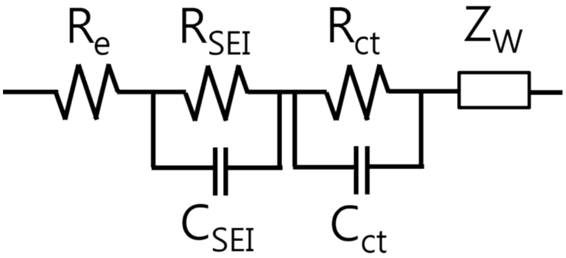

		Cycles	R_e (Ω)	R_{ct} (Ω)	R_{SEI}	Z_w (Ω)
LIB	Zn_2GeO_4	0	1	440		0.32
		3	6.3	11	3	0.37
		10	6.4	10	3	0.37
	Zn_2SnO_4	0	1	525		0.32
		3	13.9	13.6	3	0.35
		10	14.8	12.5	3	0.35
NIB	Zn_2GeO_4	0	1	600		0.45
		3	4.5	90	10	0.41
		10	4.5	83	10	0.41
	Zn_2SnO_4	0	1.3	720		0.46
		3	2.1	120	13	0.40
		10	2.1	105	13	0.40

The fitting parameter R_e represents the internal resistance (electrolyte) of the test battery, R_{ct} (and C_{ct}) is associated with the charge transfer resistance between the active materials and the electrolyte, R_{SEI} (and C_{SEI}) is associated with the resistance of the solid-electrolyte interface between the electrode and the electrolyte, and Z_W represents the Warburg impedance corresponding to the Li (or Na) ion diffusion process.

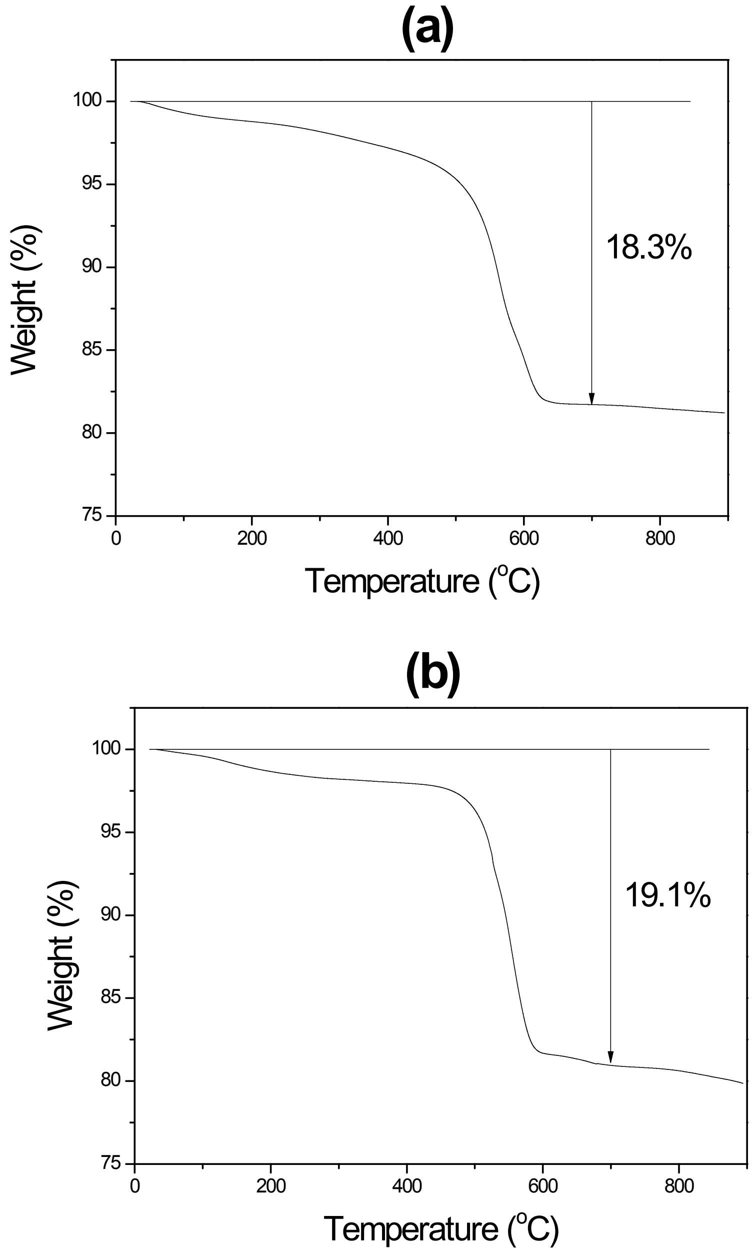

Fig. S1. TGA data showing that the C content of (a) Zn_2GeO_4- and (b) Zn_2SnO_4-graphene mixture is 18 and 19 wt. %.

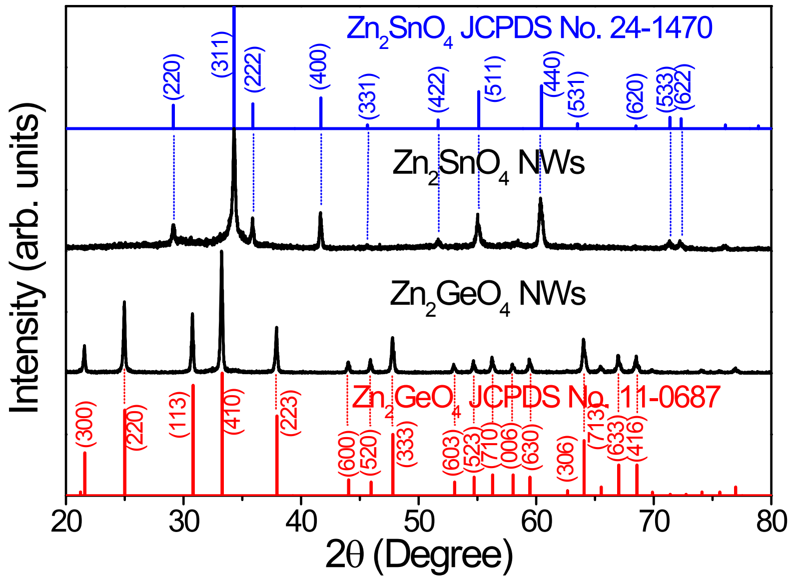

Fig. S2. Full-range XRD pattern of Zn_2GeO_4 and Zn_2SnO_4 NWs. All peaks of the Zn_2GeO_4 and Zn_2SnO_4 were well matched with those of the references; rhombohedral phase Zn_2GeO_4 (JCPDS No. 11-0687; a = 14.23 Å, c = 9.530 Å) and cubic phase Zn_2SnO_4 (JCPDS No. 24-1470; a = 8.657 Å).

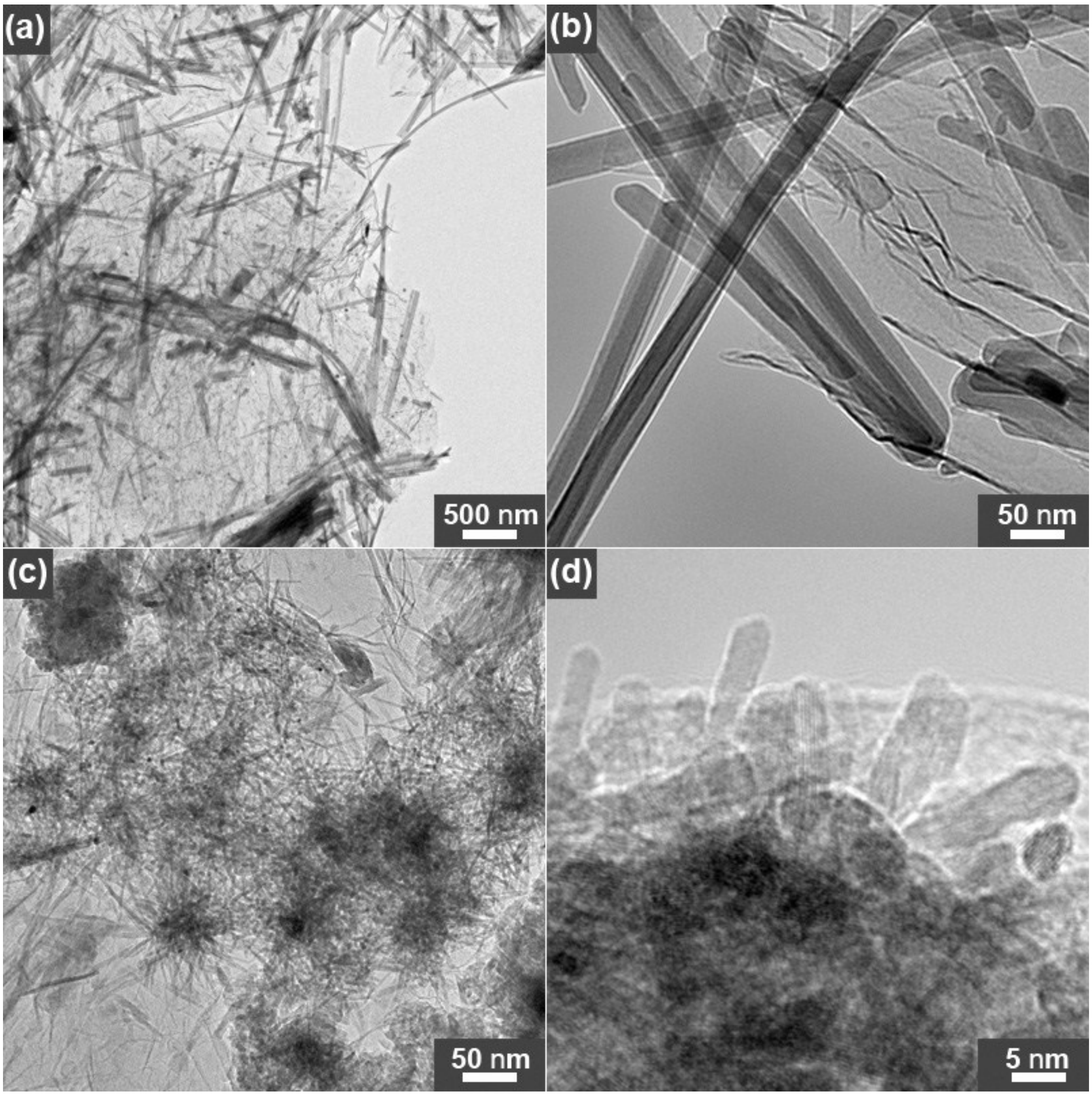

Fig. S3. TEM images for (a), (b) Zn_2GeO_4–graphene and (c), (d) Zn_2SnO_4-graphene.

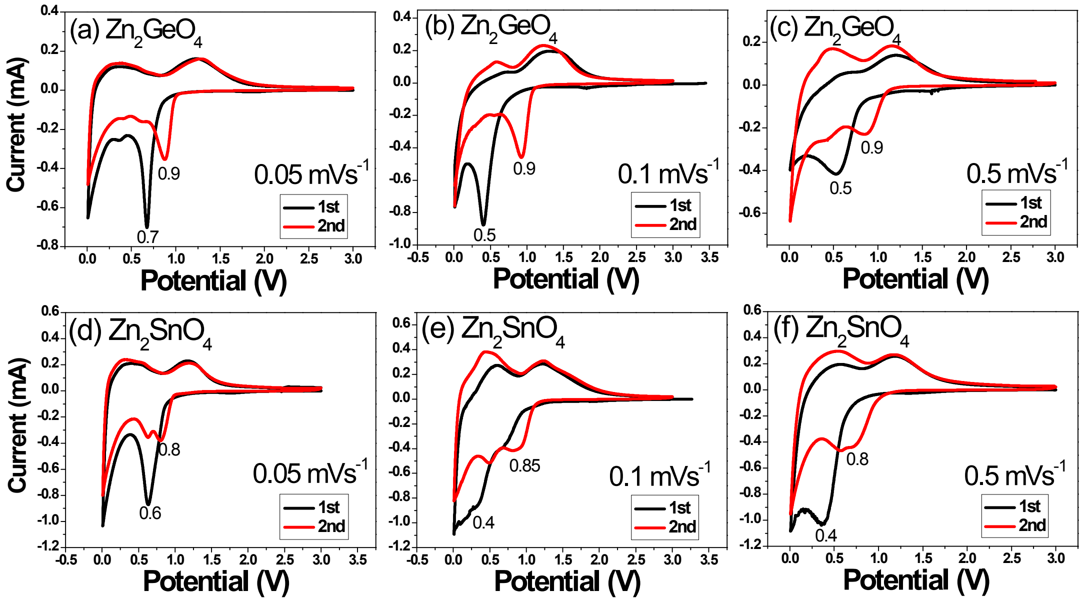

Fig. S4. Cyclic voltammetry curves; 1st and 2nd cycles of LIBs at the rate of 0.05, 0.1, and 0.5 mVs^{-1}, for (a), (b), (c) Zn_2GeO_4 and (d), (e), (f) Zn_2SnO_4. As the scan rate increases, the cathodic peak of the 1st cycle shifts to the lower voltage. This result is probably due to the kinetically unfavorable decomposition of Zn_2GeO_4 and Zn_2SnO_4: after the formation of SEI in the 1st cycle, the decomposition becomes more active at 0.8-0.9 V in the 2nd and 3rd cycles.

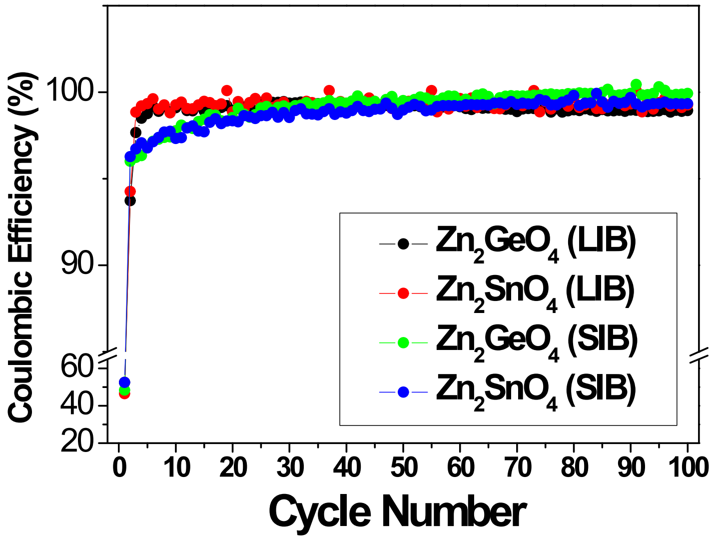

Fig. S5. Coulombic efficiency of Zn_2GeO_4 and Zn_2SnO_4 in LIBs and SIBs.

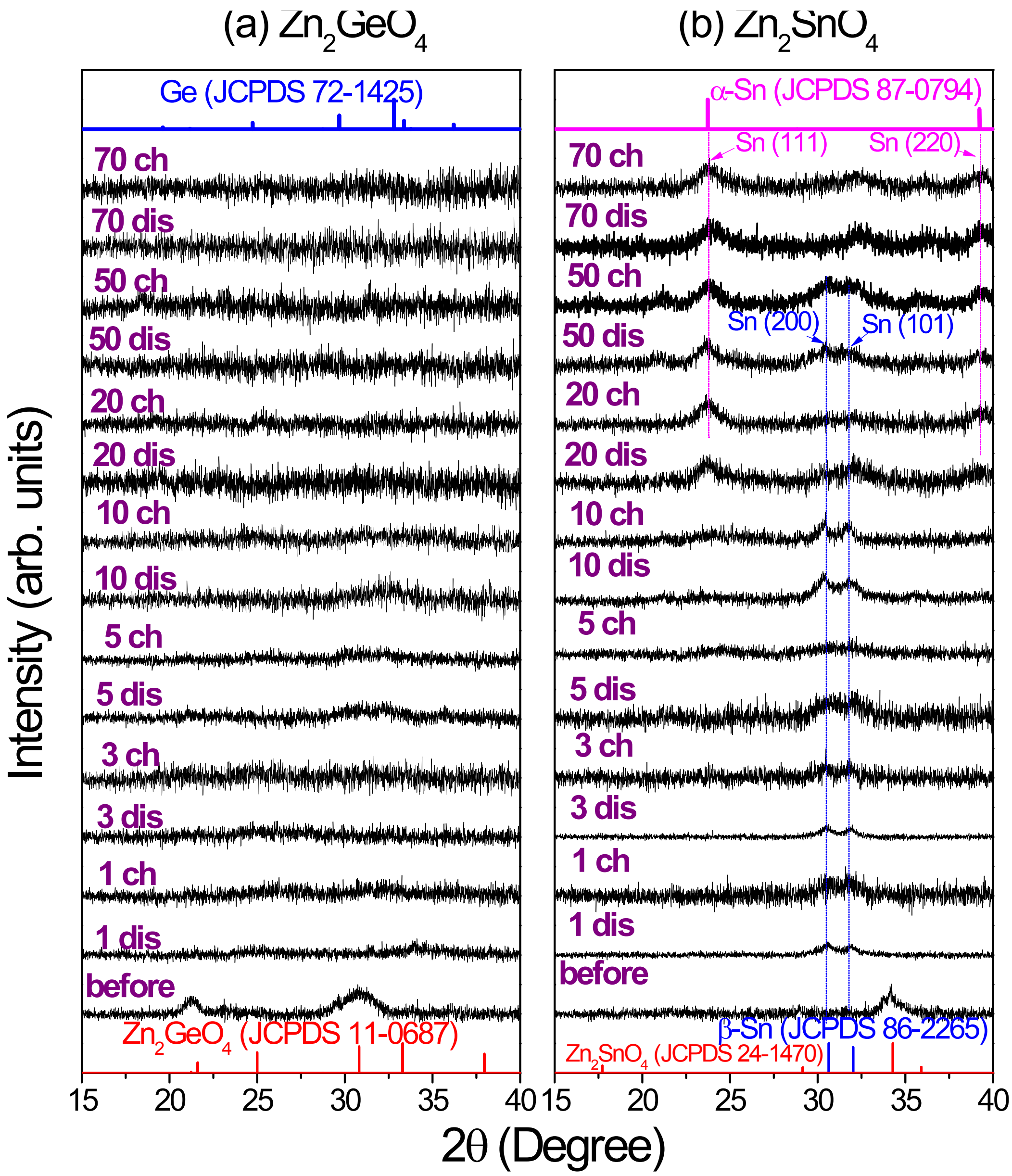

Fig. S6. *Ex situ* XRD pattern of (a) Zn_2GeO_4 and (b) Zn_2SnO_4 electrodes at charge (ch)-discharge states in LIBs. The peaks are indexed using reference XRD patterns from the appropriate JCPDS cards: rhombohedral phase Zn_2GeO_4 (JCPDS No. 11-0687; a = 14.23 Å, c = 9.530 Å), tetragonal phase Ge (JCPDS No. 72-1425; a = 5.930 Å, c = 6.980 Å), cubic phase Zn_2SnO_4 (JCPDS No.; 24-1470; a = 8.657 Å), tetragonal phase (β) Sn (JCPDS No. 86-2265; a = 5.831 Å, c = 3.181 Å), and cubic phase (α) Sn (JCPDS No. 87-0794; a = 6.489 Å). After the first discharge, all of the Zn_2GeO_4 and Zn_2SnO_4 had completely decomposed. For Zn_2GeO_4, no peaks were detected. Zn_2SnO_4 showed the formation of tetragonal phase Sn (β-Sn). As the number of cycles increased up to 20 cycles, cubic phase Sn (α-Sn) became a dominant phase.

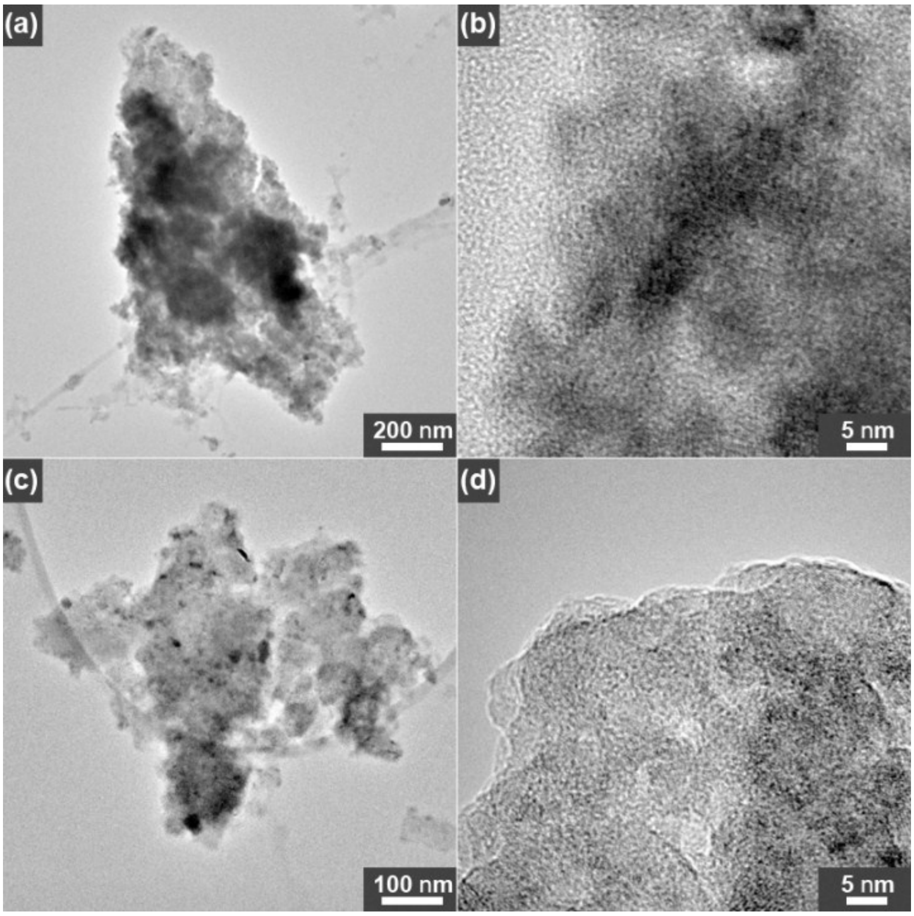

Fig. S7. HRTEM image of the Zn_2GeO_4 sample (mixed with carbon black binder and PAA) after Li extraction at (a), (b) 5^{th} and (c), (d) 70^{th} cycles. Most of crystalline NWs cracked into amorphous phase.

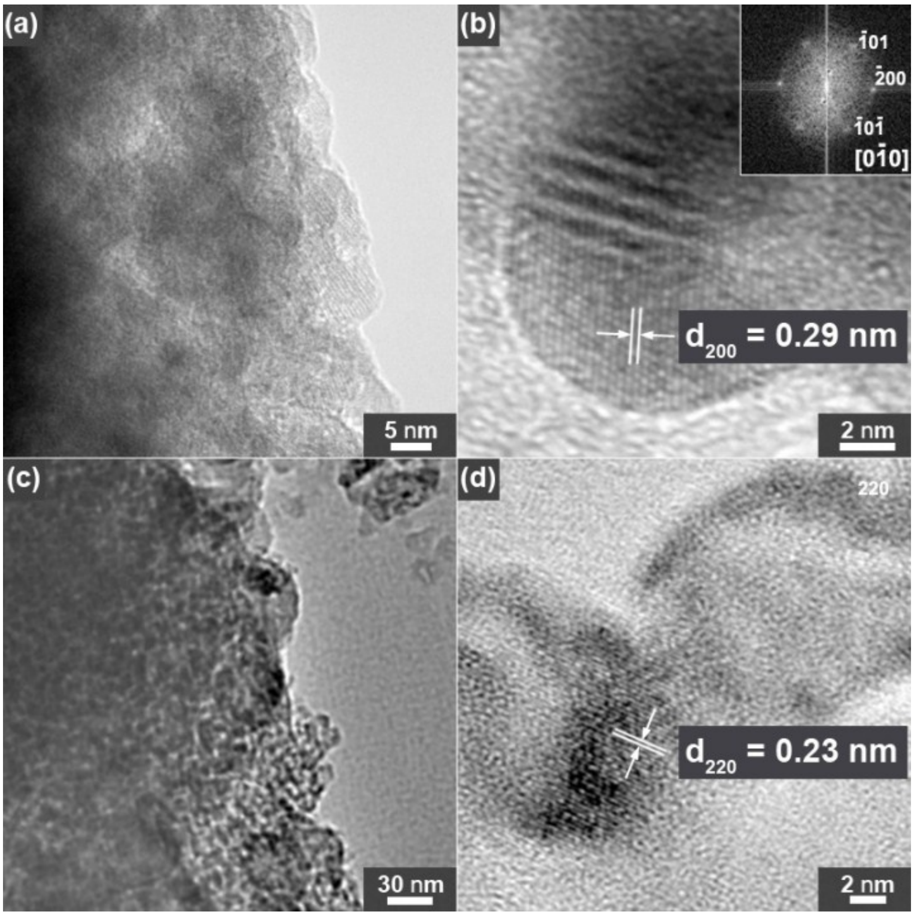

Fig. S8. HRTEM image of the Zn_2SnO_4 sample (mixed with carbon black binder and PAA) after Li extraction at (a), (b) 5^{th} and (c), (d) 70^{th} cycles. The crystalline phase remains even after 70^{th} cycles. After 5^{th} cycle, *d* spacing is identified as 2.9 Å, which corresponds to that of the (200) planes of tetragonal phase Sn (JCPDS No. 86-2265; *a* = 5.831 Å, *c* = 3.181 Å). After 70^{th} cycle, *d* spacing is identified as 2.3 Å, which corresponds to that of the (220) planes of cubic phase (α) Sn (JCPDS No. 87-0794; *a* = 6.489 Å).

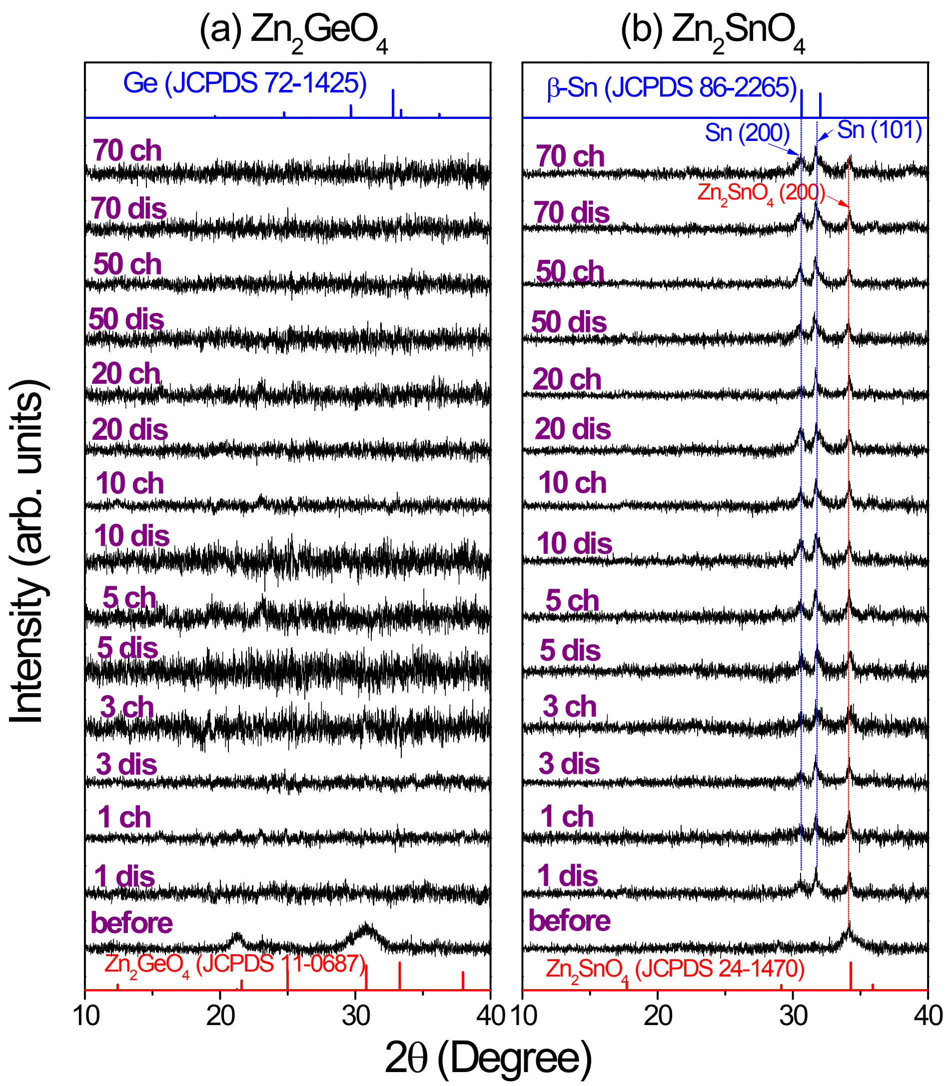

Fig. S9. *Ex situ* XRD pattern of (a) Zn_2GeO_4 and (b) Zn_2SnO_4 electrodes at charge-discharge state in SIBs. The peaks are indexed using reference XRD patterns from the appropriate JCPDS cards: rhombohedral phase Zn_2GeO_4 (JCPDS No. 11-0687; a = 14.23 Å, c = 9.530 Å), tetragonal phase Ge (JCPDS No. 72-1425; a = 5.930 Å, c = 6.980 Å), cubic phase Zn_2SnO_4 (JCPDS No.; 24-1470; a = 8.657 Å), tetragonal phase (β) Sn (JCPDS No. 86-2265; a = 5.831 Å, c = 3.181 Å). Zn_2GeO_4 NWs completely decomposed into an amorphous phase after the first discharge. Zn_2SnO_4 NWs remained up to the 70th cycle. The production of the β-Sn phase was observed upon cycling.

References

S1. J. Zeng, M. Xin, K. Li, H. Wang, H. Yan and W. Zhang, *J. Phys. Chem. C*, 2008, **112**, 4159.

S2. R. Wang, S. Wu, Y. Lv and Z. Lin, *Langmuir*, 2014, **30**, 8215.

S3. X. Zhang, L. Wang, Y. Zou, X. Peng, M. Zhang, S. GaO, J. Xu, K. Tang and D. Zhao, *Materials Letters*, 2016, **166**, 243.

S4. W. Wang, J. Qin and M. Cao, *ACS Appl. Mater. Interfaces*, 2016, **8**, 1388.

S5. H. –H. Li, L. –L. Zhang, C. –Y. Fan, X. –L. Wu, H. –F. Wang, X. –Y. Li, K. Wang, H. –Z. Sun and J. –P. Zhang, *J. Mater. Chem. A*, 2016, **4**, 2055.

S6. W. S. Yuan, Y. W. Tian and G. Q. Liu, *J. Alloy. Compd.*, 2010, **506**, 683.

S7. W. S. Yuan, Y. W. Tian and G. Q. Liu, *Russ. J. Electrochem.,* 2011, **47**, 829.

S8. K. Kim, A. Annamalai, S. H. Park, T. H. Kwon, M. W. Pyeon and M. J. Lee, *Electrochim. Acta,* 2012, **76**, 192.

S9. X. Zheng, Y. Li, Y. Xu, Z. Hong and M. Wei, *CrystEngComm*, 2012, **14**, 2112.

S10. W. Song, J. Xie, S. Liu, G. Cao, T. Zhu and X. Zhao, *J. Mater. Res.,* 2012, **27**, 3096.

S11. W. –S. Yuan, Y. –W. Tian, L. –J. Liu and J. –Z. Li, *Trans. Nonferrous Met. Soc. China*, 2012, **22**, 858.

S12. Y. Zhao, Y. Huang, Q. Wang, K. Wang, M. Zong, L. Wang, W. Zhang and X. Sun, *RSC Adv.,* 2013, **3**, 14480.

S13. Y. Zhao, Y. Huang, L. Xue, X. Sun, Q. Wang, W. Zhang and K. Wang, *Polym. Test,* 2013*,* ***32***, 1582.

S14. K Wang, Y. Huang, H. Huang, Y. Zhao, X. Qin, X. Sun and Y. Wang, *Ceram. Int.,* 2014, **40**, 8021.

S15. K. Wang, Y. Huang, T. Han, Y. Zhao, H. Huang and L. Xue, *Ceram. Int.,* 2014, **40**, 2359.

S16. X. Ji, X. Huang, Q. Zhao, A. Wang and X. Liu, *J. Nanomater.*, 2014, **2014**, 169373.

S17. K. Wang Y. Huang, Y. Shen, L. Xue, H. Huang, H. Wu and Y. Wang, *Ceram. Int.,* 2014, **40**, 15183.

S18. T. Jiang, X. Tian, H. Gu, H. Zhu and Y Zhou, *J. Alloy. Compd.*, 2015, **639**, 239.

S19. C. Yan, J. Yang, Q. Xie, Z. Lu, B. Liu, C. Xie, S. Wu, Y Zhang and Y. Guan, *Mater Lett.,* 2015, **138**, 120.

S20. S. Yuvaraj, W. J. Lee, C. W. Lee and R. K. Selvan, *RSC Adv.*, 2015, 5, 67210.

S21. L. Qin, S. Liang, A. Pan and X. Tan, *Mater Lett.*, 2016, **164**, 44.